ENDF-266
TREE-1259

FISSION PRODUCT AND REACTOR DOSIMETERY STUDIES
AT
COUPLED FAST REACTIVITY MEASUREMENTS FACILITY

March 1978

EG&G Idaho, Inc.

IDAHO NATIONAL ENGINEERING LABORATORY

DEPARTMENT OF ENERGY

IDAHO OPERATIONS OFFICE UNDER CONTRACT EY-76-C-07-1570

FISSION PRODUCT AND REACTOR DOSIMETRY STUDIES
AT
COUPLED FAST REACTIVITY MEASUREMENTS FACILITY

By
Y. D. Harker
J. W. Rogers
D. A. Millsap

Compiled by
Y. D. Harker

EG&G IDAHO, INC.

MARCH 1978

ACKNOWLEDGMENTS

ABSTRACT

The Coupled Fast Reactivity Measurements Facility (CFRMF) plays a
special role in the Idaho National Engineering Laboratory's general
program to provide basic technological data for the development of fission
reactors as safe and economical sources of energy for domestic use.
Because of its unique features the CFRMF has been used to provide key
integral data in the areas of fast neutron fission product capture effects
and fast reactor dosimetry development. This report has been prepared to
provide in one document a specification of the CFRMF and the results of
measurements performed in it. The data are expected to be used in the
evaluation and testing of neutron cross-section files pertaining to
fission products, dosimetry materials, and other special applications.

CONTENTS

FIGURES

TABLES

FISSION PRODUCT AND REACTOR DOSIMETRY STUDIES
AT
COUPLED FAST REACTIVITY MEASUREMENT FACILITY

I. INTRODUCTION

Nuclear data are used to support design and operation of reactor systems in the following ways:

1. establishing criteria for core and shielding design,
2. defining long-range fissile material requirements,
3. predicting and optimizing reactor system performance,
4. establishing requirements for nuclear waste processing.

Since the development of nuclear energy began, there have been programs in basic nuclear data measurements to provide and improve nuclear data in support of the advancement of nuclear power. Because the requirements and degree of sophistication in nuclear power development are continuing to advance as the industry matures, it is necessary to continue to maintain forward-looking programs in base technology development. The physics programs at the Idaho National Engineering Laboratory (INEL) are a part of this national effort in base technology development.

The information and data presented in this report represent the culmination of a particular phase in base technology development in the areas of:

1. cross-section data pertaining to fission-product-class nuclides,
2. reaction-rate data for materials utilized in reactor dosimetry.

In this report integral neutron-cross-section and reaction-rate data obtained from measurements performed in the Coupled Fast Reactivity Measurement Facility (CFRMF) are presented. Because the CFRMF neutron spectrum spans the intermediate neutron energy range (1 keV $\leq E_n \leq 1$ MeV) and is "a typical fast reactor type spectrum," integral cross-section and reaction-rate data obtained in this neutron field are important to base technology development pertaining to fast reactors. Principal activities involving measurements in the CFRMF are concerned with capture effects in fission product nuclides, reaction-rate determinations in selected dosimetry materials, and capture and fission effects in actinide nuclides.

1

Fission products are a class of nuclides which contain
the largest number of nuclides for which nuclear data are desired and
for which the least is known about the values of the neutron cross sections
in the intermediate-neutron-energy range. The neutron capture effect
due to the presence of these nuclides in the reactor fuel is known to
be a very important factor in limiting the lifetime of the fuel. Such
a limitation has a direct effect on the economics of the reactor operation.
Secondly, the presence of these nuclides is a serious consideration in
the handling and processing of irradiated fuel.

Reactor dosimetry has a significant part in evaluating reactor
performance and in analyzing experiments related nuclear fuel damage.
Dosimetry technology is being advanced through a coordinated multi-
laboratory effort called the Interlaboratory LMFBR Reaction Rate (ILRR)
program. In this program, reaction-rate measurements are being per-
formed in well characterized neutron fields in the U. S. and Europe.
Samples irradiated in these fields are analyzed by participating labora-
tories and the results are intercompared first to assess the state-of-
the art in determining reaction rates and second to improve on dosimetry
methods. The CFRMF was selected as the first facility to be used in
this program, and because of its well characterized neutron environ-
ment and its ability to operate at moderate flux levels (up to 10^{12}
n/cm^2-sec), it has been the most extensively used facility in the ILRR
program.

Integral cross-section and reaction-rate data obtained from measure-
ments in the CFRMF are used in evaluating and testing cross section
information to be included or already contained in the Evaluated Nuclear
Data File (ENDF/B). Evaluation and testing is performed by members of
the Cross Section Evaluations Working Group (CSEWG) which is a multi-U.S.-
laboratory effort coordinated through the National Nuclear Data Center
(NNDC) of Brookhaven National Laboratory (BNL). Personnel involved in
the INEL physics programs are members of this working group. Part of
our CSEWG committment is to provide supporting documentation to maintain
the CFRMF as a "benchmark" for integral testing data contained in ENDF/B
The issuance of this report is a part of our committment to CSEWG and
also to the ILRR.

2

The following areas are covered:

1. A physical description of the CFRMF and its control system are presented. In this section a brief description is given of the CFRMF which is sufficient to provide a suitable assessment of the facility for data evaluation and testing purposes. Greater detail concerning the facility and the extensive characterization program conducted in it are contained in the references [1-5].

2. A specification of the CFRMF suitable for R-Z transport calculations is contained. This specification is provided to assist anyone who undertakes to perform a transport calculation.

3. Results of capture cross-section measurements on selected fission-product nuclides are presented. Fifty-two reactions involving fission-product nuclides are presented along with brief descriptions of sample configurations.

4. Results of reaction-rate measurements on dosimetry materials are presented. These data were obtained through the ILRR program and are presented in this report so that such data may be used to evaluate dosimetry cross-section data and to establish the degree of characterization achieved for the CFRMF.

5. As stated earlier, an extensive characterization program for the CFRMF has been in progress and part of this effort has been the use of reactor physics calculations. Reported in this section is the neutron spectrum derived from one-dimensional calculations using multi-group transport theory and ENDF/B IV cross section data. This spectrum is recommended for use in data testing; however, a new recommended spectrum will be presented for each new version of ENDF/B.

3

II. PHYSICAL DESCRIPTION OF THE CFRMF

The Coupled Fast Reactivity Measurements Facility (CFRMF) at the
Idaho National Engineering Laboratory (INEL) is a zoned-core critical
assembly with a fast-neutron spectrum zone in the center of an enriched
^{235}U, water-moderated thermal "driver," and the core is contained in a
large pool about 4.5 m beneath the surface. The concept, preliminary
considerations, and most details of the CFRMF have been documented[1-5].
The CFRMF was originally designed as a high-precision static-reactivity
measurements facility operating at a flux level of approximately 10^8 neu-
trons per square centimetre per second (n/cm^2·s), but has more recently
found much use in the fast breeder reactor program as a fast-neutron field
for the irradiation of materials of interest at flux levels up to approxi-
mately 10^{12} n/cm^2·s.

Figure 1 is a cutaway pictorial diagram of the CFRMF. As shown in
Figure 2, which is a midplane cross-sectional diagram of the CFRMF, the
core has quadrantal symmetry with respect to structural assembly and
fuel loading. The thermal driver zone fuel elements are conventional
plate elements of aluminum-clad, fully enriched (approximately 93%)
^{235}U. The fueled portion of the core is 60.96 cm long, and each element
is 8.183 cm square. The fast zone is so constructed that it is kept
water-free and so that it can be used to "filter" or "tailor" the neutron
energy spectrum. Figure 3 is a horizontal midplane cross-sectional
diagram of the fast zone assembly. The 0.317-cm-thick stainless steel
housing has a water-free seal and is only thick enough to provide the
strength necessary to support the large mass of uranium. The 0.635-cm-
thick 50 wt% boral side and end plates completely shroud the assembly
except that each boral end plate has a centered hole 4.20 cm in diameter,
through which the experiment access tube passes. Outside each boral end
plate is a 2.697-cm-thick aluminum spacer through which the access tube
also extends. The lower aluminum plate positions the uranium block; the
upper plate provides symmetry.

The ^{238}U (99.7%) block (14.52 cm square x 60.69 cm long and weighing
approximately 217 kg) with a 5.295-cm hole drilled through its axial

4

Sample Entry Tube

Fuel Elements

U^{235}

B^{10}

U^{238}

Boral
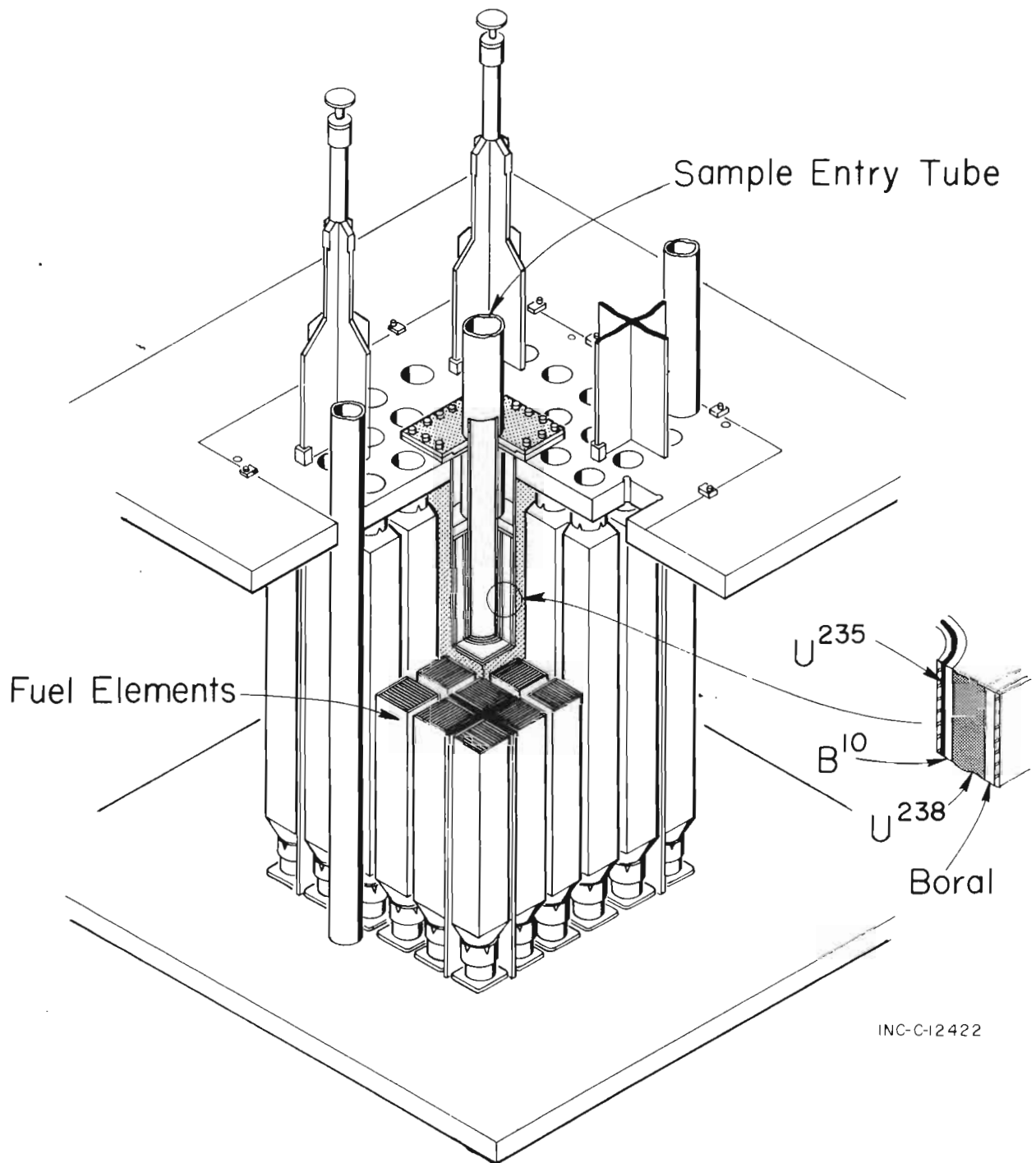
INC-C-12422

Fig. 1 Cutaway pictorial diagram showing general assembly of
the CFRMF.

5
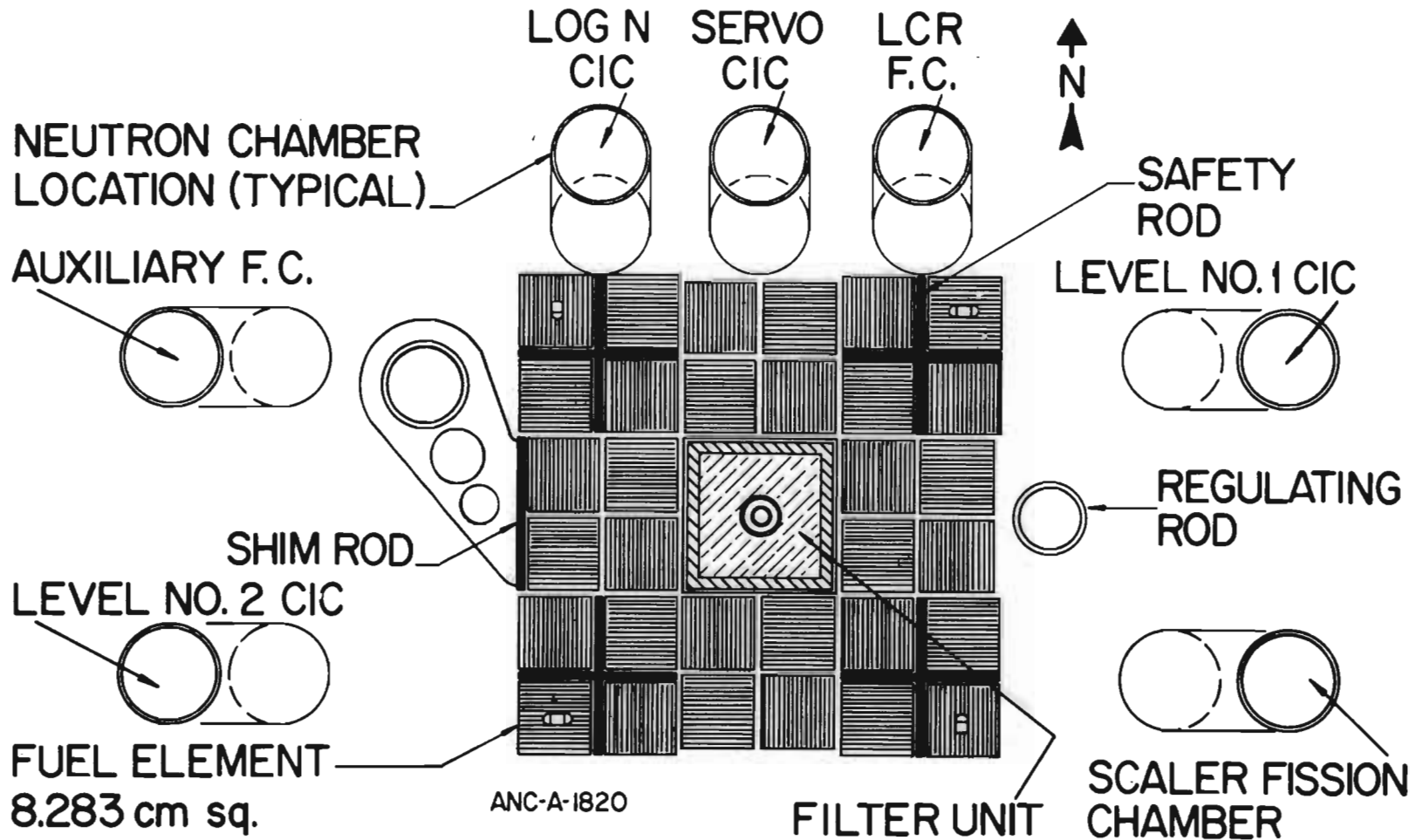
CFRMF CORE

Fig. 2. Midplane cross-sectional diagram of CFRMF core, control deveices, and chamber locations.

ANC-A-1820

FILTER UNIT

STAINLESS STEEL HOUSING

^{238}U BLOCK   STAINLESS STEEL ACCESS TUBE

BORAL PLATES

^{10}B^{10} ANNULUS

^{235}U ANNULUS

EXPERIMENT AREA

ANC-A-1821
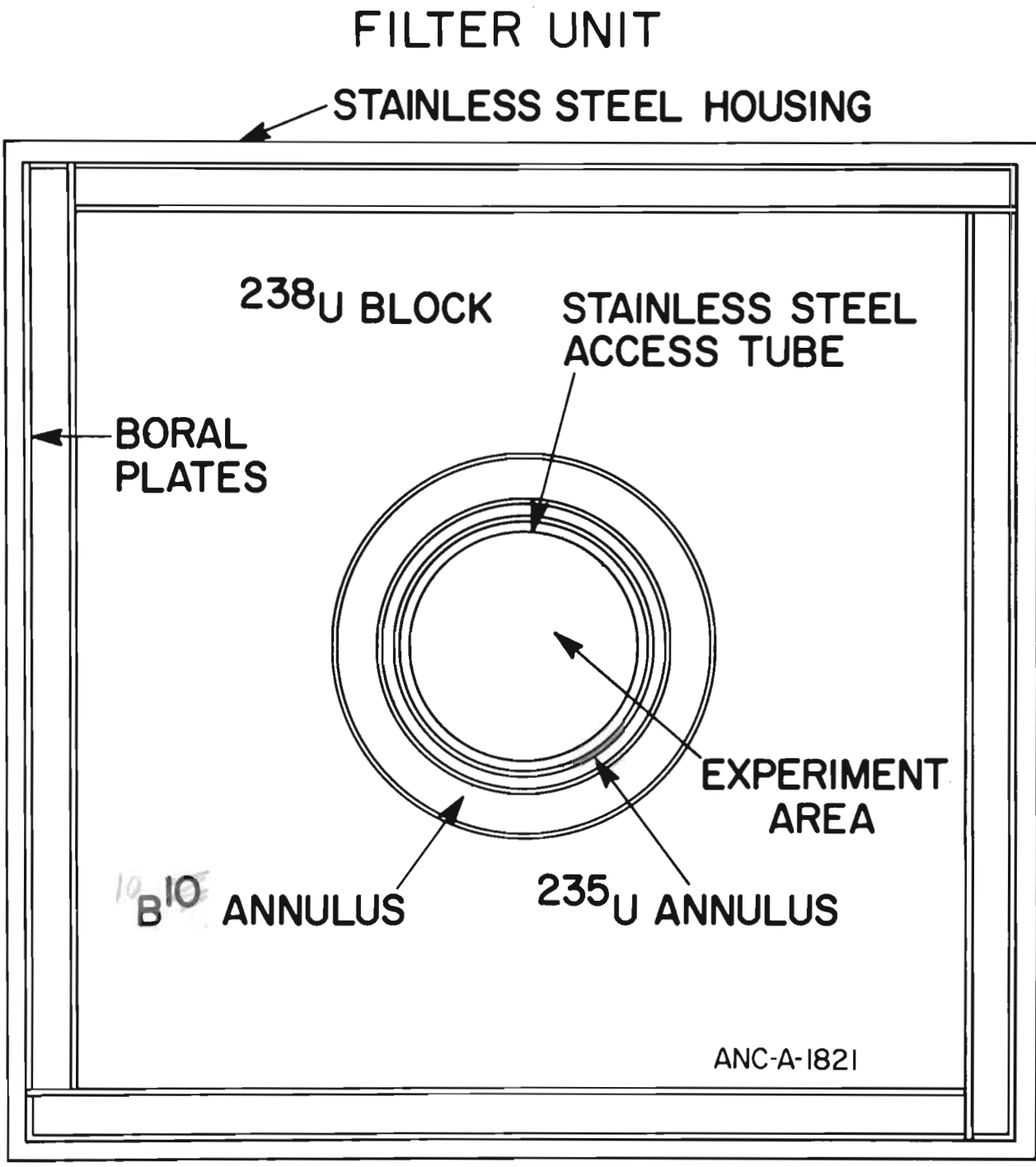
Fig. 3. Midplane cross-sectional diagram of filter unit which forms the CFRMF fast zone.

center is vertically aligned with the core fuel. The 0.635-cm-thick annulus of enriched ^{10}B (90%) and 0.0889-cm-thick annulus of enriched ^{235}U (93%) are clad with 0.0305-cm-thick stainless steel and they slip-fit together into the ^{238}U block. The ^{235}U and ^{238}U materials are solid metal, and the stainless steel is either Type 304 or 321. The ^{10}B is crystalline powder and is vibrocompacted to a density of 1.355 g/cm^3. The stainless steel access tube, with 0.147-cm-thick walls in the core region, slip-fits inside the ^{235}U annulus and will accept objects with effective diameters up to 3.78 cm. The distance from the bottom of the access tube to the core midplane is 31.11 cm; it is approximately 6.1 m from the core midplane to the top of the access tube above the pool surface. Asymmetry exists in the fast zone vertical plane because above the top aluminum spacer is a 15.75-cm cube-shaped void capped with a 2.54-cm-thick stainless steel cover plate through which the access tube passes. Below the bottom aluminum spacer is the 1.27-cm-thick stainless steel end plate of the housing, which rests on the aluminum-grid support structure of the reactor, with a metal-to-water ratio of approximately 0.6 by volume.

The materials in the fast zone assembly filter or tailor the thermal neutron energy spectrum of the driver zone in the following general manner. The boron in the boral plates attenuates the neutrons below approximately 1 keV by absorption. The ^{238}U block degrades the energy of the fission neutrons by inelastic scattering. The ^{10}B annulus attenuates the neutrons below approximately 1 keV even further and ensures that all thermal neutrons are removed. The ^{235}U annulus has no significant effect on the real flux spectrum other than supplying some fast-fission neutrons, but this annulus does affect the importance function (adjoint flux) which is of concern in reactivity measurements.

When the CFRMF functions as a high-precision irradiation facility, the power-level control system must reproducibly establish the desired neutron level and energy spectrum without changing the flux distribution at the location of the experiment. Control device locations are shown in Figure 2. The safety rods are not used for normal operation control
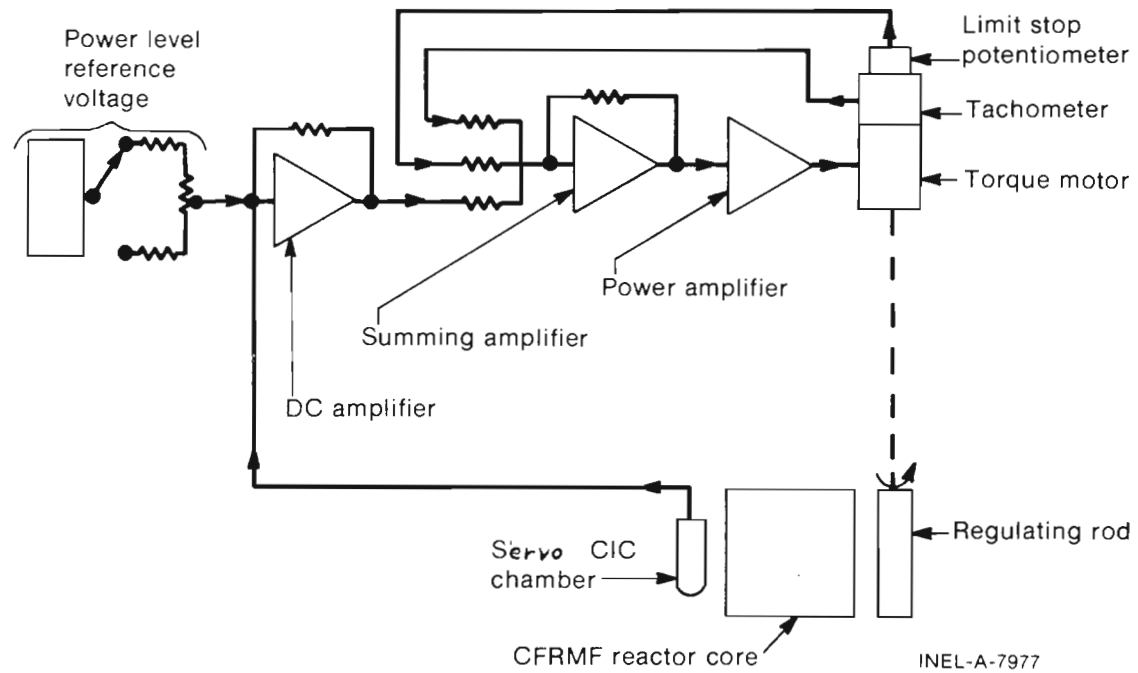
Fig. 4.   CFRMF power level control servo system used for maintaining a fixed neutron level.

purposes and are completely out-of-core during irradiations. The shim rod, a 1-mm-thick, 15.24-cm x 60.96-cm cadmium plate on a flat surface parallel to the core, is always set at the same position for related irradiations and can be repositioned to within $\pm 5 \times 10^{-4}$ of a degree of rotation (equivalent to 1.5×10^{-7} $\Delta k/k$), which causes no detectable changes in the flux distribution in the experiment region.

The power of the CFRMF is maintained at a constant and preset level by means of a conventional dc servo system, shown in Figure 4. This servo system is composed of a boron-lined compensated ion chamber (CIC). appropriate amplifiers, a reference voltage source, and a torque motor-driven regulating rod (a 1-mm-thick, 6.0-cm x 60.96-cm cadmium plate on a curved surface 6.35 cm in diameter and parallel to the core). The signal applied to the first-stage amplifier is the difference between a current proportional to the reactor power level as produced by the servo CIC and a current obtained from the reference voltage source. The power-level error signal is then amplified and used to drive the regulating rod to correct for any power-level deviation. The regulating rod is capable of holding the power level steady with a total motion corresponding to a reactivity of $\pm 8.4 \times 10^{-8}$ $\Delta k/k$ at low power levels, where thermal heating causes no problems. At the power levels normally used for irradiations, the reactivity changes observed are approximately 1×10^{-4} $\Delta k/k$; such changes also do not produce detectable changes in the in-core flux distribution. The servo CIC, reference voltage, and first-state dc amplifier determine the reproducibility and linearity of multiples of the power level. The servo CIC positioning reproducibility has been measured to $<\pm 0.5\%$. During long-term (several years) observations, chambers such as the CFRMF servo CIC in neutron fields equal to or greater than that of the CFRMF have been so stable that no changes in stability have been detected. Routine checks ensure that the compensation and bias voltages of the servo CIC are stable and at the proper levels.

The reference voltage unit, which is used to preset the level at which the power is controlled, consists of a voltage power supply potentio-meter and two switchable precision resistors (100x and 1000x). The

10

stability of this device is ±0.01% or better over the normal ambient temperature range. The linearity of the CFRMF power level control system has been checked against foil activiations and fission rates in the fast zone center. A factor-of-10 change (0.6 to 6.0 kW) on the power level setpoint produces a change of 9.6 or a nonlinearity of 4%. This nonlinearity, however, is reproducible and stable. Measurements of the reference voltage supply output at each of these setpoints shows no more than 1% nonlinearity for each range of the system. Consequently, the nonlinearity of the power level control system is likely due to imperfect CIC compensation.

III. CFRMF DIMENSIONAL SPECIFICATIONS FOR
NEUTRONIC CALCULATIONS

1. IMPORTANCE OF DIMENSIONAL SPECIFICATIONS

The central measurement position of the Coupled Fast Reactivity Measurements Facility (CFRMF) at the INEL is being used to obtain a variety of integral measurement data (reaction rates, reactivities, etc.) for reactor materials of interest to the Liquid Metal Fast Breeder Reactor and other fast reactor programs. Accurate knowledge of the neutron spectrum in the measurement position of the CFRMF is of major importance in the analysis of these data. In order to provide this knowledge an extensive program of spectrum measurements and calculations was initiated during the construction of the facility and has continued until the present. Because measurement techniques, cross-sectional evaluations, and reactor physics codes are continually being refined and improved, a sizeable effort in measurements and calculations is maintained in order to give the most up-to-date characterization possible of the central spectrum of the CFRMF.

During design and critical loading of the core, efforts were made to retain transverse and axial symmetry. However, practical limitations have necessitated certain departures from this ideal. Because of these departures from symmetry, radial and axial measurements and calculations must be made in order to determine the magnitude and nature of any effects that existing asymmetry may have on the spectrum in the central measurement position. In this section, we present, as accurately as possible, the dimensional specifications necessary to making r,z calculations for the study of axial flux distributions in the central spectrum of the CFRMF.

2. THE CALCULATIONAL MODEL

Since the CFRMF thermal driver zone and several important fast zone structures are rectangular in shape, it is impossible to give an exact r,z representation of the reactor. Furthermore there are sufficient

structural complexities that even a cylindrical version of the trans-
verse dimensions requires considerable homogenization in order to make
a calculation practicable. The calculational model presented here has
homogenized most of the thermal driver region, and gives a fuel composition
which preserves the masses of uranium, aluminum, and water actually present
in the reactor. However, it should be noted that in fact the core contains
fuel elements in the driver with six different fuel compositions. This
homogenization of the fuel region will therefore give a somewhat inaccurate
source distribution in the driver. This will affect the eigenvalue but
should not bias axial flux distributions to any appreciable extent. The
fast zone is, however, more explicitly represented. The axial representa-
tion has included all pertinent features above and below the core both for
the fast region and the thermal driver zone which might influence the
axial flux distributions of the central measurement position.

The details of the r,z calculational model are given in Tables I
through V. Table I lists the dimensions of the interfaces used to define
the regions of the model and their coded number designations (arabic
numerals for the radial direction, roman numerals for axial direction).
To identify each region numerically, the combined number of the axial
and radial interfaces forming the upper left-hand boundary of each region
is used to designate that region. Figure 5, the reactor model, shows this
clearly. In this figure, which is not drawn to scale, all regions are
represented as either simple cylinders or cylindrical shells.

Table II is a tabulation of the various regions in the model,
including a brief description of the reactor components contained in
each region, and the code number for the composition contained in each
region. Table II is a tabulation of the various regions in the model,
including a brief description of the reactor components contained in
each region. Table III gives the volume fractions of the various materials
contained in each composition code. Table IV lists the elements or iso-
topes contained in each of the materials along with their atom densities
and the parameters used to calculate those atom densities. The material
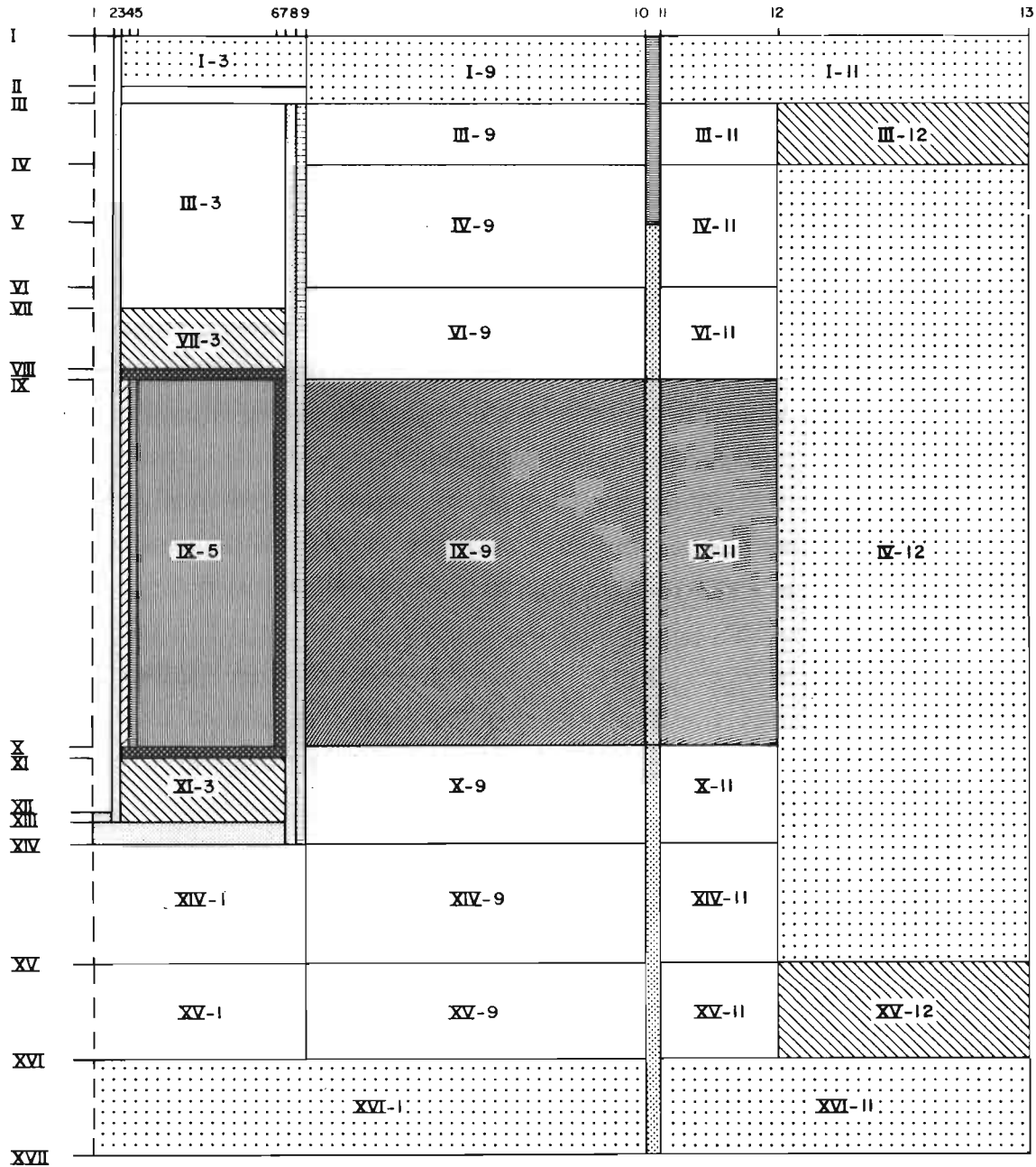
Fig. 5. Diagram of CFRMF r,z Calculational Model
(Not drawn to scale)

14

atom densities given were calculated by the relation

$$N = \rho \frac{M}{M_T} \frac{N_A}{A} \tag{1}$$

where

N = material atom density (atom/cm^3)

ρ = material density (g/cm^3)

M/M_T = elemental or isotopic mass divided by the total mass of the material

N_A = Avogadro's number (atoms/mole)

A = atomic weight of the element or isotope g/mole).

When a composition atom density rather than material atom density is desired, the results of the expression above must be multiplied by the respective volume fractions given in Table III. If an isotope occurs in more than one material of a particular composition, then the composition atom density for that isotope is found by adding the material atom densities weighted by the appropriate volume fractions.

3. INFORMATION FOR FURTHER CALCULATIONS

If more calculations for resonance and/or thermal cross sections are desired, refer to the information given in Table V where additional information for the fuel element plates and the heavily shielded compositions is given. Figure 6 aids in interpreting the information given in the table.
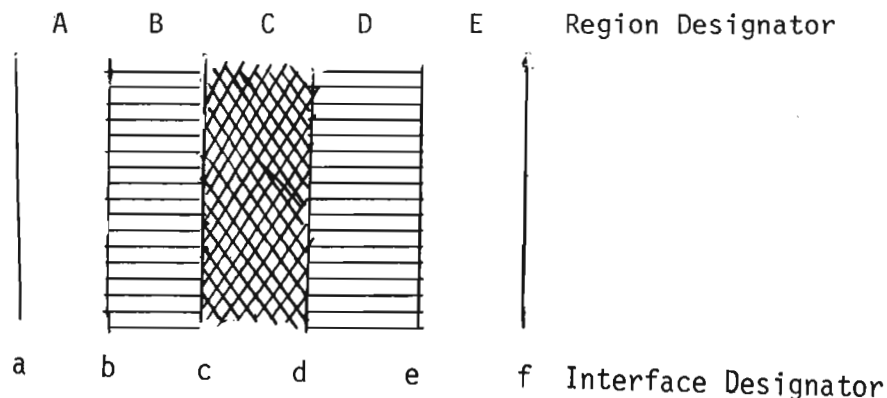
Fig. 6 Generalized Diagram for Clad Regions

15

For crosschecks, other information may also be of use. The material volume fractions given in Table III can be derived from the data given in Table V for composition numbers 3, 4, 6, and 8b; but the dimensional data for compositions 3 and 4 are for cylindrical shells, while compositions 6 and 8b are for slabs (as is 18.). Composition 8b is that of a single fuel plate. There are 15 plates in each fuel element and 32 fuel elements in the core. The cross-sectional area occupied by each fuel element is 69.4512 cm^2. Total fuel loading is 5698.9 g U-235 (93.16% enriched). The total cross-sectional area of the four cruciform-shaped safety rods is 86.2837 cm^2. The area of the assembly to the reflector is equivalent to 36 fuel elements plus the area of the safety rods. The weight of en-riched uranium in the U-235 sleeve is 1494.7 g, and the weight of enriched boron in the 10_B sleeve is 437.05 g.

TABLE I

rz MODEL DIMENSIONS

Interface Number	r (cm)	Δr(cm)
1	0.0	--
2	1.91643	1.91643
3	2.06375	0.14732
4	2.25996	0.19621
5	2.69748	0.43752
6	8.19129	5.49381
7	8.97084	0.77955
8	9.39210	0.42126
9	9.40362	0.01152
10	23.03407	13.63045
11	23.62263	0.58866
12	28.69351	5.07078
13	43.69351	15.00

Interface Number	z (cm)	Δz (cm)
I	0.0	--
II	9.04875	9.04875
III	11.58875	2.54
IV	16.66875	5.08
V	21.035	4.36625
VI	26.035	5.00
VII	27.14625	1.11125
VIII	29.845	2.69875
IX	30.48	0.635
X	91.44	60.96
XI	92.075	0.635
XII	94.059375	1.984375
XIII	94.77375	0.7143758
XIV	95.885	1.11125
XV	105.25125	9.36625
XVI	112.87125	7.62

TABLE II

REGION SPECIFICATIONS

Region Number	Description	Composition Number
I-1	Measurement Hole	1
I-2	Dry Tube Wall	2
IX-3	Uranium Sleeve	3
IX-4	Boron-10 Sleeve	4
IX-5	Depleted Uranium Block	5
IX-6	Boral Liner (Sides)	6
III-7	Fast Assembly Containment Vessel (sides)	2
III-8	Water Annulus	7
IX-9	Homogenized Reactor Fuel (Or Side Plates and Homogenized Fuel Plates)	8 (Or 8a & 8b)
IX-10	Safety Rod Followers (Core Section)	9
IX-11	Homogenized Reactor Fuel	8
IV-12	Reflector	7
XII-1	Bottom of Dry Tube	2
VIII-3	Boral Liner (Top)	6
X-3	Boral Liner (Bottom)	6
VII-3	Spacer Block (Top)	10
XI-3	Spacer Block (Bottom)	10
III-3	Empty Space	1
II-3	Fast Assembly Containment Vessel (Top)	2
XIII-1	Fast Assembly Containment Vessel (Bottom)	2
VI-9	Ends of Fuel Elements (Top, Inner)	11
V-10	Safety Rod Followers (Above Core)	19
VI-11	Ends of Fuel Elements (Top, Outer)	11
X-9	Ends of Fuel Elements (Bottom, Inner)	11
X-10	Safety Rod Followers (Below Core)	19
X-11	Ends of Fuel Elements (Bottom, Outer)	11
IV-9	Fuel Element Adapters & End Boxes (Top, Inner)	12
IV-11	Fuel Element Adapters & End Boxes (Top, Outer)	12
XIV-1	Special Adapters & Vessel Positioning Pins	13
XIV-9	Fuel Element Adapters & End Boxes (Bottom, Inner)	14
XIV-11	Fuel Element Adapters & End Boxes (Bottom, Outer)	14

18

TABLE II (Continued)

Region Number	Description	Composition Number
III-9	Grid (Top, Inner)	15
III-11	Grid (Top, Outer)	15
III-12	External Portion of Grid (Top)	10
XV-1	Grid Below Fast Assembly	16
XV-9	Grid (Bottom, Inner)	17
XV-11	Grid (Bottom, Outer)	17
XV-12	External Portion of Grid (Bottom)	10
I-3	Reflector	7
I-9	Reflector	7
I-10	Safety Rods	18
I-11	Reflector	7
XVI-1	Reflector	7
XVI-II	Reflector	7

TABLE III

COMPOSITION SPECIFICATIONS

Composition Number	Material Number	Description	Volume Fraction
1	1	Void	1.0
2	2	Stainless Steel, Type 304	1.0
3	1	Void	0.19337
	2	Stainless Steel, Type 304	0.31988
	3	Enriched Uranium (Sleeve)	0.48675
4	1	Void	0.0557
	2	Stainless Steel, Type 304	0.1443
	4	Enriched Boron Powder	0.8000
5	5	Depleted Uranium	1.0
6	1	Void	0.08088
	6	Boral Core Material (50 wt% B C in Al)	0.61765
	7	Aluminum	0.30147
7	8	Water	1.0
8*	7	Aluminum	0.27445
	8	Water	0.62501
	9	Enriched Uranium (in an aluminum Matrix)	0.10053
8a*	7	Aluminum	0.94358
	8	Water	0.05642
8b*	7	Aluminum	0.18287
	8	Water	0.70284
	9	Enriched Uranium (in an Al Matrix)	0.11429
9	7	Aluminum	0.4340
	8	Water	0.5660
10	7	Aluminum	1.0
11	7	Aluminum	0.3682
	8	Water	0.6318
12	7	Aluminum	0.1227
	9	Water	0.6734
	10	Stainless Steel, Type 17-4 PH	0.2039
13	7	Aluminum	0.2257
	8	Water	0.5802
	10	Stainless Steel, Type 304	0.1941
14	7	Aluminum	0.1227
	8	Water	0.6516
	10	Stainless Steel, Type 17-4 PH	0.2257

TABLE III (Continued)

Composition Number	Material Number	Description	Volume Fraction
15	7	Aluminum	0.5505
	8	Water	0.3547
	10	Stainless Steel, Type 17-4 PH	0.0948
16	7	Aluminum	0.4283
	8	Water	0.5717
17	7	Aluminum	0.5205
	8	Water	0.4163
	10	Stainless Steel, Type 17-4 PH	0.0632
18	7	Aluminum	0.6057
	8	Water	0.2470
	11	Cadmium	0.1473
19	7	Aluminum	0.7530
	8	Water	0.2470

* Composition Number 8 contains 12.039% 8a (fuel element side plates) and 87.961% 8b (Homogenized fuel plates).

TABLE IV

MATERIAL SPECIFICATIONS

Material Number	Material Density (g/cm^3)	ENDF/B Number	Element or Isotope	Elemental or Isotopic Mass Fraction	Elemental or Isotopic Mass (gm/mole) (Carbon-12 Scale)	Atom Density (Atoms/cm^3 x 10^{-24}) N = 6.022045 x 10^{23}
1	--	--	--	--	--	--
2	7.92	1190	Nickel	0.0913	58.71	0.00742
		1191	Chromium	0.1804	51.996	0.01656
		1192	Iron	0.7072	55.847	0.06040
		1194	Silicon	0.0044	28.086	0.00075
		1197	Manganese-55	0.0160	54.938	0.00139
			Other	0.0006	--	--
3	18.9	1034	Uranium-234	0.0100	234.041	0.00049
		1261	Uranium-235	0.93115	235.044	0.04509
		1163	Uranium-236	0.00415	236.046	0.00020
		1262	Uranium-238	0.0547	238.051	0.00262
4	1.3152	1273	Boron-10	0.9071	10.0129	0.07175
		1160	Boron-11	0.0929	11.0093	0.00668
5	18.876	1261	Uranium-235	0.00193	235.044	9.334-5
		1262	Uranium-238	0.99782	238.051	0.04765
			Other	0.00025	--	--
6	2.61	1273	Boron-10	0.07748	10.0129	0.01216
		1160	Boron-11	0.31384	11.0093	0.04481
		1274	Carbon	0.10868	12.011	0.01422
		1193	Aluminum	0.5	26.9815	0.02913
7	2.699	1193	Aluminum	1.0	26.9815	0.06024

TABLE IV (Continued)

Material Number	Material Density (g/cm^3)	ENDF/B Number	Isotope	Isotopic Mass Fraction	Isotopic Mass (g/mole) (Carbon-12 Scale)	Atom Density (Atoms/cm^3 x 10^{-24}) N = 6.022045 x 10^{23}
8	0.998595 (18°C)	1269	Hydrogen	0.111894	1.0079	0.06676
		1276	Oxygen	0.888106	15.9994	0.03338
9	3.0840	1192	Aluminum	0.85437	26.9815	0.058808
		1034	Uranium-234	0.00150	234.041	1.190-5
		1261	Uranium-235	0.13567	235.044	1.0720-3
		1163	Uranium-236	0.00029	236.046	2.282-6
		1262	Uranium-238	0.00817	238.051	6.374-5
10	7.78	1190	Nickel	0.0425	58.71	0.00339
		1191	Chromium	0.1700	51.996	0.01532
		1192	Iron	0.7365	55.847	0.06187
		1194	Silicon	0.0050	28.086	0.00083
		1197	Manganese-55	0.0050	54.938	0.00043
		1295	Copper	0.0400	63.546	0.00295
			Other	0.0010	--	--
11	8.62	1281	Cadmium	1.0	112.40	0.04618

23

TABLE V-A

DETAILED SPECIFICATIONS FOR SELECTED COMPOSITIONS (CYLINDRICAL GEOMETRY)

Region Designator	Material Number	Description	Thickness of Annulus (cm)	Interface Designator	Radius In Core (cm)
Uranium-235 Sleeve (Composition No 3)					
A	1	Void	0.02777	a	2.06375
B	2	Stainless Steel, Type 304	0.03340	b	2.09152
C	3	Enriched Uranium	0.09504	c	2.12492
D	2	Stainless Steel, Type 304	0.02921	d	2.21996
E	1	Void	0.01079	e	2.24917
				f	2.25996
Boron-10 Sleeve (Composition No. 4)					
A	1	Void	0.01080	a	2.25996
B	2	Stainless Steel, Type 304	0.02921	b	2.27076
C	4	Enriched Boron Powder	0.35052	c	2.29997
D	2	Stainless Steel Type 304	0.03364	d	2.65049
E	1	Void	0.01335	e	2.68413
				f	2.69748

TABLE V-B

DETAILED SPECIFICATIONS FOR SELECTED COMPOSITIONS (SLAB GEOMETRY)

Region Designator	Material Number	Description	Thickness of Slab (cm)
Boral (Composition No. 6)			
A	1	Void	0.02794
B	7	Aluminum	0.10414
C	6	Boral Core Material	0.42672
D	7	Aluminum	0.10414
E	1	Void	0.02794
Typical Fuel Plate (Composition No. 8b)			
A	8	Water	0.19524
B	7	Aluminum	0.05080
C	9	Enriched Uranium (in Al)	0.06350
D	7	Aluminum	0.05080
E	8	Water	0.19524
Typical Safety Rod Blade (Related to Composition No. 18)			
A	8	Water	0.07620
B	7	Aluminum	0.19050
C	11	Cadmium	0.10160
D	7	Aluminum	0.19050
E	8	Water	0.07620

25

IV. FISSION PRODUCT CAPTURE
CROSS SECTIONS

Fission product capture sections have been measured by activation
techniques using the Coupled Fast Reactivity Measurements Facility CFRMF)
as the irradiation source. A description of the CFRMF and the characteri-
zation of its neutron field is given in Section II and References 1-5.
Activation measurements are performed by exposing a well-characterized
sample along with flux monitors to the neutron environment in the test
region of the CFRMF. Reaction rates are thus derived by measuring the
activity of the reaction products by means of gamma spectroscopy. Run-
to-run normalization and normalization relative to a standard are des-
cribed in the following subsection.

1. SOME NOTES ON RESULTS

The results of these measurements are summarized in Table VI. No
self-shielding corrections have been made to the data; the table includes
a brief description of each sample, however, so that such corrections
can be made if desired. Calculated integrals based on ENDF/B IV fission
product data and the spectrum (SCAMP 75/271) given in Section V are also
included in the table. Once again, no attempt has been made to account
for sample self-shielding in the calculations.

Error estimates are included with the measured reaction rates. These
estimates include all uncertainties contributing to the uncertainty of
determining a reaction rate from an irradiation experiment of this type.
The major contribution to the error in each case is the estimated un-
certainty associated with the decay data of each reaction product. At
this time, the errors are conservative estimates based on a preliminary
review of the decay data used. Future review of the literature is
expected to alter these estimates.

In the majority of comparisons between measured and calculated
reaction rates, the measured values are smaller than the respective

calculated values. In many cases the differences are of a magnitude which suggests self-shielding effects. There will be further study to determine the magnitude of self-shielding for a selected set of reactions.

From Table VI it appears that agreement between measurements and calculations is in the range of 10-25%. In Section V, similar comparisons are presented for materials (reactions) utilized in reactor dosimetry. There the overall agreement is in the range of 5%. This agreement substantiates that the activation method is capable of accuracies of at least this magnitude when the data used in analysis (primarily decay parameters) are of sufficient quality. If, therefore, the decay data for the reaction products are improved through additional measurements or improved evaluations, the accuracy of the data presented here will benefit.

2. NORMALIZATION OF ACTIVATION
DATA

Each irradiation experiment performed in the CFRMF for the purpose of measuring fission product capture by activation utilized at least one gold flux monitor foil (0.127) mm thick). In early activation experiments in the CFRMF, gold capture was considered the standard to which all activation measurements would be referenced. Relative reaction rates were determined on this basis by dividing the saturated reaction rate of the reaction under study by the gold monitor saturated reaction rate associated with that measurement.

As a result of this program's involvement in the Interlaboratory LMFBR Reaction Rate (ILRR) program, improved techniques of standardization became available, one of which was the determination of the integrated flux of the CFRMF using multifoil dosimetry. This technique uses the gold flux monitors associated with each experiment to provide run-to-run normalization, which can then be traced to an ILRR experiment for which an integrated flux was determined. Using this approach, spectral

27

average cross sections were determined by dividing the measured saturated reaction rate of the reaction under study by the integrated flux level determined for that irradiation.

Further study revealed that using gold as a standard and relying on dosimetry-determined integrated fluxes is inferior to using the fission rate of ^{235}U as the standard. As a result of CFRMF involvement in the ILRR program this rate has been determined to a high degree of accuracy ($\sim$ 1%) using a National Bureau of Standards fission chamber. On an absolute basis this measured rate is many times more accurate than the rate measured for gold capture or for the integrated flux determined from multifoil dosimetry measurements. Another advantage of using ^{235}U(n,f) as a standard is that the calculated spectral average fission cross section for the CFRMF neutron spectrum is much less dependent on the spectral shape chosen. Thus the conversion of the measured relative reaction rates to absolute spectral average cross sections using [$\sigma_f^{(235}U)$] calc. is not as dependent on spectrum as the same procedure using [$\sigma_c^{(197}Au)$] calc. or the conversion using the flux derived from multifoil dosimetry. For these reasons, it was decided to convert all activation data to a ^{235}U(n,f) standard. The following steps describe the method by which this conversion was accomplished.

1. The gold monitors used in the ILRR irradiations were thinner (0.0508 mm) and located differently than the gold monitors used in our activation measurements involving fission products. Thus an experiment was performed to correlate the results obtained from the two types of monitor configurations. The results of that correlation run are

ILRR Gold Monitor

reaction rate = 4.785 x 10^{-14} captures/sec atom ($\pm$ 0.06%)   (2)

Activation Gold Monitor

reaction rate = 4.859 x 10^{-14} capture/sec atom ($\pm$ 0.31%)   (3)

$$\text{RATIO: } \frac{\text{Fission Products Monitor}}{\text{ILRR Monitor}} = 1.015 \; (\pm \; 0.31\%) \qquad (4)$$

2. From the ILRR data the following parameters have been determined:

$$\Phi \; \sigma_f(^{235}U) \; = \; 1.221 \times 10^{-13} \text{ fissions/sec·atom } (\pm \; 1.4\%). \qquad (5)$$

A reaction rate for ILRR Au monitor =

$$3.008 \times 10^{-14} \text{ capture/sec·atom } (\pm \; 1.0\%) \qquad (6)$$

3. Based on items 1 and 2, the fission product flux level monitor data are converted to ^{235}U fission rates by applying the relationship

$$\Phi \; \sigma_f(^{235}U) = 4.00 \times [\text{Fission Products Gold Monitor Capture Rate}] \; (\pm \; 1.7\%). \quad (7)$$

4. For those data recorded relative to gold capture, the following relationship is applied to convert to $^{235}U(n,f)$ standard:

$$\frac{\Phi \; \sigma_c(A,Z)}{\Phi \; \sigma_f(^{235}U)} = \frac{\left[\dfrac{\Phi \; \sigma_c(A,Z)}{\Phi \; \sigma_c(^{197}Au)} \right].}{4.00(\pm \; 1.7\%)} \qquad (8)$$

TABLE VI

FISSION PRODUCT REACTION RATE

Reaction	Sample Description	Sample Mass	$\hat{\sigma}_c(A,Z) / \hat{\sigma}_f(235,92)$ Measured[a]	Calculated[b]	Measured/Calculated
^{87}Rb(n,γ)^{88}Rb	RbCl powder in a disk shape 1 cm diameter x 1.6 mm thick	62.6 mg	$8.50 \times 10^{-3}(\pm 12\%)$	7.46×10^{-3}	1.14
^{89}Y(n,γ)^{90m}Y	Metal chips		$2.20 \times 10^{-4}(\pm 7.7\%)$	- - -	- - -
^{93}Nb(n,γ)^{94m}Nb	Nb Metal foil .79 cm square x .13 mm thick	69 mg	$1.15 \times 10^{-1}(\pm 50\%)$	7.65×10^{-2}	1.50
^{99}Tc(n,γ)^{100}Tc	Tc powder in a disk shape 1 cm diameter x 1.6 mm thick	99.2 mg	$1.72 \times 10^{-1}(\pm 11\%)$	1.74×10^{-1}	.99
^{98}Mo(n,γ)^{99}Mo	Mo metal foil $\approx$1 cm diameter x 0.13 mm thick	99.0 mg	$3.81 \times 10^{-2}(\pm 11\%)$	4.36×10^{-2}	.87
^{100}Mo(n,γ)^{101}Mo	Mo metal foil 1 cm diameter x 0.13 mm thick	99.0 mg	$2.24 \times 10^{-2}(\pm 8.7\%)$	3.11×10^{-2}	.72
^{102}Ru(n,γ)^{103}Ru	Ru powder in a disk shape 1 cm diameter x 1.6 mm thick	87.5 mg	$5.55 \times 10^{-2}(\pm 8.1\%)$	7.84×10^{-2}	.71
^{104}Ru(n,γ)^{105}Ru	Ru powder in a disk shape 1 cm diameter x 1.6 mm thick	75.4 mg	$5.18 \times 10^{-2}(\pm 6.3\%)$	5.50×10^{-2}	.94
^{103}Rh(n,γ)^{104m}Rh	Rh wire 0.254 mm dia-meter	6.3 mg per cm length	$2.02 \times 10^{-2}(\pm 12\%)$	- - -	- - -

TABLE VI (Continued)

Reaction	Sample Description	Sample Mass	$\hat{\sigma}_c(A,Z)$ / $\hat{\sigma}_f(235,92)$ Measured[a]	Calculated[b]	Measured/Calculated
^{103}Rh(n,γ)^{104g}Rh	Rh wire 0.254 mm diameter	6.3 mg per cm length	2.15×10^{-1}($\pm$ 26%)	- - -	- - -
^{103}Rh(n,γ)^{104}Rh	- - -	$\sum =$	2.35×10^{-1}($\pm$ 24%)	2.64×10^{-1}	.89
^{107}Ag(n,γ)^{104g}Ag	Ag metal foil $\approx$ 1 cm diameter x .13 mm thick	100 mg	2.75×10^{-1}($\pm$ 15%)	2.65×10^{-1}	1.04
^{109}Ag(n,γ)^{119g}Ag	Ag metal foil $\approx$ 1 cm diameter x .13 mm thick	100 mg	3.11×10^{-1}($\pm$ 12%)	- - -	- - -
^{109}Ag(n,γ)^{119m}Ag	Ag metal foil $\approx$ 1 cm diameter x .13 mm thick	100 mg	1.80×10^{-2}($\pm$ 6.6%)	- - -	- - -
^{109}Ag(n,γ)^{110}Ag	- - -	$\sum =$	3.29×10^{-1}($\pm$ 11%)	1.92×10^{-1}	1.71
^{108}Pd(n,γ)^{109}Pd	Pd metal foil $\approx$ 1 cm diameter x .13 mm thick	98.1 mg	7.81×10^{-2}($\pm$ 25%)	- - -	- - -
^{110}Pd(n,γ)^{111}Pd	Pd metal foil $\approx$ 1 cm diameter x .13 mm thick	98.1 mg	3.06×10^{-3}($\pm$ 10%)	- - -	- - -
^{115}In(n,γ)^{116m}In	In metal foil .13 mm thick	63.7 mg	1.67×10^{-1}($\pm$ 7.9%)	1.92×10^{-1}	.94
^{121}Sb(n,γ)^{122}Sb	Sb powder in a disk shape 1 cm diameter x 1.6 mm thick	132.1 mg	1.74×10^{-1}($\pm$ 6.3%)	1.93×10^{-1}	.90

31

TABLE VI (Continued)

32

Reaction	Sample Description	Sample Mass	$\hat{\sigma}_c(A,Z) / \hat{\sigma}_f(235,92)$ Measured[a]	Calculated[b]	Measured/Calculated
$^{123}Sb(n,\gamma)^{124}Sb$	Sb powder in a disk shape 1 cm diameter x 1.6 mm thick	132.1 mg	$9.65 \times 10^{-2} (\pm 8.9\%)$	1.05×10^{-1}	.92
$^{127}I(n,\gamma)^{128}I$	AgI powder evenly distributed over 1 cm x 1.5 cm area	(^{127}I) 5.51 mg	$1.85 \times 10^{-1} (\pm 19\%)$	2.14×10^{-1}	.86
$^{128}I(n,\gamma)^{130}I$	$Ag^{129}I$ powder evenly distributed over 1 cm x 1.5 cm area	(^{129}I) 5.29 mg	$1.14 \times 10^{-1} (\pm 8.6\%)$	1.46×10^{-1}	.78
$^{132}Xe(n,\gamma)^{133m}Xe$	^{132}Xe implanted in Al foil over area 13.1 cm x 5 cm	(^{132}Xe) 286.8 µg	$1.52 \times 10^{-3} (\pm 15\%)$	- - -	- - -
$^{132}Xe(n,\gamma)^{133g}Xe$	^{132}Xe implanted in Al foil over area 13.1 cm x 5 cm	(^{132}Xe) 286.8 µg	$2.45 \times 10^{-2} (\pm 8.0\%)$	- - -	- - -
$^{132}Xe(n,\gamma)^{133}Xe$	- - -	$\sum =$	$2.60 \times 10^{-2} (\pm 7.6\%)$	- - -	- - -
$^{134}Xe(n,\gamma)^{135}Xe$	^{134}Xe implanted in Al foil over area 13.2 cm x 5 cm	(^{134}Xe) 106.0 µg	$9.29 \times 10^{-3} (\pm 6.6\%)$	1.51×10^{-2}	.61
$^{133}Cs(n,\gamma)^{134m}Cs$	Cs_2SO_4 powder in a disk 1 cm diameter x 1.6 mm thick	69.6 mg	$3.47 \times 10^{-2} (\pm 16\%)$	- - -	- - -
$^{133}Cs(n,\gamma)^{134}Cs$	$CsNO_3$ powder in bottom of quartz vial-hemispherical 6.4 mm diameter	9.01 mg	$1.72 \times 10^{-1} (\pm 6.4\%)$	1.89×10^{-1}	.91

TABLE VI (Continued)

Reaction	Sample Description	Sample Mass	$\sigma_c(A,Z) / \sigma_f(235,92)$ Measured[a]	Calculated[b]	Measured/Calculated
$^{150}Nd(n,\gamma)^{151}Nd$	Nd_2O_3 powder in a disk 1 cm diameter x 1.6 mm thick	60.82 mg	$6.02 \times 10^{-2}(\pm 21\%)$	9.15×10^{-1}	.66
$^{152}Sm(n,\gamma)^{153}Sm$	Sm_2O_3 powder in a disk 1 cm diameter x 1.6 mm thick	87.39 mg	$1.82 \times 10^{-1}(\pm 4.9\%)$	1.88×10^{-1}	.97
$^{154}Sm(n,\gamma)^{155}Sm$	Sm_2O_3 powder in a disk 1 cm diameter x 1.6 mm thick	87.39 mg	$7.33 \times 10^{-1}(\pm 4.5\%)$	9.78×10^{-1}	.75
$^{151}Eu(n,\gamma)^{152m1}Eu$ ($I_{\frac{1}{2}}$ = 9.3h)	$^{151}Eu_2O_3$ powder in hemispherical bottom of quartz vial (6.4 mm diameter) 4 mm deep	15.33 mg	$6.75 \times 10^{-1}(\pm 8.4\%)$	- - -	- - -
$^{151}Eu(n,\gamma)^{152m2}Eu$ ($I_{\frac{1}{2}}$ = 96 m)	$^{151}Eu_2O_3$ powder in polyethylene container	15.49 mg	$1.39 \times 10^{-3}(\pm 9.5\%)$	- - -	- - -
$^{151}Eu(n,\gamma)^{152g}Eu$	$^{151}Eu_2O_3$ powder in hemispherical bottom of quartz vial (6.4 mm diameter) 4 mm deep		——————		
$^{151}Eu(n,\gamma)^{152}Eu$	- - -	$\sum$ =	$1.64 (\pm 6.3\%)$	1.43	1.15
$^{153}Eu(n,\gamma)^{154}Eu$	$^{153}Eu_2O_3$ powder in hemispherical bottom of quartz vial (6.4 mm diameter) 4 mm deep	14.87 mg	$9.49 \times 10^{-1}(\pm 7.9\%)$	8.90×10^{-1}	1.07
$^{158}Gd(n,\gamma)^{159}Gd$	Gd metal foil 1 cm diameter x 0.051 mm thick	30 mg	$1.12 \times 10^{-1}(\pm 12\%)$	1.15×10^{-1}	.98

33

TABLE VI (Continued)

Reaction	Sample Description	Sample Mass	$\hat{\sigma}_c(A,Z) / \hat{\sigma}_f(235,92)$ Measured[a]	Calculated[b]	Measured/Calculated
^{133}La(n,γ)^{140}La	La$_2$O$_3$ powder in a disk 1.27 cm diameter x 3.2 mm thick	416 mg	1.14 x 10^{-2}(± 6.3%)	- - -	- - -
^{140}Ce(n,γ)$^{1-1}$Ce	CeO$_2$ powder in a disk 1.27 cm diameter x 3.2 mm thick	431 mg	5.45 x 10^{-4}(± 8.7%)	8.71 x 10^{-3}	.063
^{142}Ce(n,γ)^{143}Ce	CeO$_2$ powder in a disk 1.27 cm diameter x 3.2 mm thick	431 mg	1.16 x 10^{-2}(± 11%)	1.56 x 10^{-2}	.74
^{141}Pr(n,γ)^{142}Pr	Pr powder in a disk 1 cm diameter x 1.6 mm thick	79.8 mg	4.75 x 10^{-2}(± 10%)	6.39 x 10^{-2}	.74
^{147}Pm(n,γ)^{143m}Pm	^{147}Pm$_2$O$_3$ powder evenly distributed over 1 cm diameter area	13.6 mg	2.21 x 10^{-1}(± 13%)	- - -	- - -
^{147}Pm(n,γ)^{148g}Pm	^{147}Pm$_2$O$_3$ powder evenly distributed over 1 cm diameter area	13.6 mg	2.69 x 10^{-1}(± 18%)	- - -	- - -
^{147}Pm(n,γ)^{148}Pm	- - -	$\sum$ =	4.90 x 10^{-1}(± .12%)	4.87 x 10^{-1}	1.01
^{146}Nd(n,γ)^{147}Nd	Nd$_2$O$_3$ powder in a disk 1.25 cm diameter x 1.7 mm thick	84.63 mg	4.15 x 10^{-2}(± 14%)	5.72 x 10^{-2}	.72
^{148}Nd(n,γ)^{149}Nd	Nd$_2$O$_3$ powder in a disk 1 cm diameter x 1.6 mm thick	60.82 mg	6.67 x 10^{-2}(± 9.1%)	1.02 x 10^{-1}	.66

34

TABLE VI (Continued)

Reaction	Sample Description	Sample Mass	$\bar{\sigma}_c(A,Z) / \bar{\sigma}_f(235,92)$ Measured[a]	Calculated[b]	Measured/Calculated
$^{160}Gd(n,\gamma)^{161}Gd$	Gd metal foil 1 cm diameter x 0.051 mm thick	30 mg	$5.75 \times 10^{-2} (\pm 8.5\%)$	8.97×10^{-2}	.64
$^{169}Tm(n,\gamma)^{170}Tm$	Tm metal foil .13 mm thick	78 mg	$2.93 \times 10^{-1} (\pm 12\%)$	- - -	- - -
$^{181}Ta(n,\gamma)^{182m}Ta$	Ta metal foil .05 mm thick	142.05 mg	$4.70 \times 10^{-4} (\pm 22\%)$	- - -	- - -
$^{181}Ta(n,\gamma)^{182g}Ta$	Ta metal foil .05 mm thick	142.05 mg	$3.29 \times 10^{-1} (\pm 9.0\%)$	- - -	- - -
$^{181}Ta(n,\gamma)^{182}Ta$	- - -	$\sum =$	$3.29 \times 10^{-1} (\pm 9.0\%)$	3.46×10^{-1}	.95
$^{186}W\ (n,\gamma)^{187}W$	W metal foil .127 mm thick	258 mg	$9.00 \times 10^{-2} (\pm 13\%)$	- - -	- - -

[a] $\bar{\sigma}_f(235,92)$ was measured using a National Bureau of Standards fission chamber; run-to-run normalization is based on gold flux monitors included with each irradiation run.

{b] Calculated rations are based on ENDF/B IV cross-section data. The neutron spectrum used in obtaining spectral averages was derived from one-dimension transport theory (SCAMP-72/271) from ENDF/B IV data (section VI).

$[\sigma_f(235,92)]$ calc. = 1.595 barn/atom.

V. DOSIMETRY REACTION RATE
MEASUREMENTS AND CALCULATIONS

Integral reaction rates have been obtained for fissionable and non-fissionable dosimeter materials irradiated in the CFRMF neutron field. Fission chamber, solid-state track recorder, gamma-ray spectrometry, and helium mass spectrometry measurements and analysis techniques were used to determine these reaction rates. Several laboratories were involved in the planning, preparation, and execution of these measurements; the results presented here represent the efforts of many people associated with these laboratories. Table VII summarizes the measured reaction rates in CFRMF at the 6-kW power level, which corresponds to 7.9×10^{10} n/cm$^2 \cdot$sec($\pm$ 1.9%).

Using the calculated neutron spectrum from Section V, reaction rates have been calculated for all measured reaction rates. Table VIII lists these reaction rates relative to the ^{235}U fission rate and compares them by ratios of measured to calculated rates.

TABLE VII

CFRMF MEASURED REACTION RATES

Reaction	Reaction Rate [reactions/ sec·atom)] $\times 10^{15}$	
$^{235}U(n,f)$	122.1	$\pm$ 1.4%
$^{238}U(n,f)$	5.96	$\pm$ 1.9%
$^{239}Pu(n,f)$	142.3	$\pm$ 1.6%
$^{237}Np(n,f)$	43.5	$\pm$ 1.9%
$^{45}Sc(n,\gamma)^{46}Sc$	1.845	$\pm$ 1.8%
$^{58}Fe(n,\gamma)^{59}Fe$	0.481	$\pm$ 1.5%
$^{59}Co(n,\gamma)^{60}Co$	7.197	$\pm$ 2.3%
$^{63}Cu(n,\gamma)^{64}Cu$	3.56	$\pm$ 4.5%
$^{115}In(n,\gamma)^{116m}In$	22.1	$\pm$ 2.5%
$^{197}Au(n,\gamma)^{198}Au$	33.3	$\pm$ 1.0%
$^{238}U(n,\gamma)^{239}U$	$17.5^{[a]}$	$\pm$ 2.4%
$^{27}Al(n,\gamma)^{24}Na$	0.0127	$\pm$ 1.2%
$^{27}Al(n,p)^{27}Mg$	0.0687	$\pm$ 2.0%
$^{46}Ti(n,p)^{46}Sc$	0.205	$\pm$ 2.0%
$^{47}Ti(n,p)^{47}Sc$	0.328	$\pm$ 4.0%
$^{48}Ti(n,p)^{48}Sc$	0.00541	$\pm$ 2.0%
$^{54}Fe(n,p)^{54}Mn$	1.371	$\pm$ 1.0%
$^{58}Ni(n,p)^{58}Co$	1.900	$\pm$ 1.0%
$^{115}In(n,n')^{115m}In$	3.90	$\pm$ 4.4%
$^{6}Li(n, \text{total } ^{4}He)$	76.07	$\pm$ 1.0%
$^{10}B(n, \text{total } ^{4}He)$	145.8	$\pm$ 1.6%

[a] Corrected for resonance self-shielding

TABLE VIII

COMPARISON OF MEASURED AND CALCULATED REACTION RATES IN CFRMF

Reaction	Measured[a]	Calculated	Measured/Calculated
$^{235}U(n,f)$	1.00 (Ref.)	1.00 (Ref.)	1.00 (Ref.)
$^{238}U(n,f)$	0.0488	0.0481	1.014
$^{239}Pu(n,f)$	1.165	1.117	1.043
$^{237}Np(n,f)$	0.356	0.363	0.981
$^{45}Sc(n,\gamma)^{26}Sc$	0.0151	0.0126	1.198
$^{58}Fe(n,\gamma)^{59}Fe$	0.00394	0.00386	1.021
$^{59}Co(n,\gamma)^{60}Co$	0.0589	0.0566	1.041
$^{63}Cu(n,\gamma)^{64}Cu$	0.0292	0.0299	0.977
$^{115}In(n,\gamma)^{116m}In$	0.181	0.190	0.953
$^{197}Au(n,\gamma)^{198}Au$	0.273	0.261	1.046
$^{238}U(n,\gamma)^{239}U$	0.144[b]	0.146	0.987
$^{27}Al(n,\alpha)^{24}Na$	0.000104	0.000111	0.937
$^{27}Al(n,p)^{27}Mg$	0.000563	0.000590	0.954
$^{46}Ti(n,p)^{46}Sc$	0.00168	0.00143	1.175
$^{47}Ti(n,p)^{47}Sc$	0.00269	0.00321	0.838
$^{48}Ti(n,p)^{48}Sc$	0.0000443	0.0000274	1.617
$^{54}Fe(n,p)^{54}Mn$	0.0112	0.0111	1.009
$^{58}Ni(n,p)^{58}Co$	0.0156	0.0148	1.054
$^{115}In(n,n')^{115m}In$	0.0319	0.0300	1.063
$^{6}Li(n, total \ ^{4}He)$	0.623	0.608	1.025
$^{10}B(n, total \ ^{4}He)$	1.194	1.064	1.122

[a] Relative to ^{235}U fission rate. Spectral averaged cross sections can be obtained by multiplying listed values by $\sigma_f(92.235) = 1.595$ barns/atom.

[b] Corrected for resonance self-shielding.

38

VI. THEORETICAL CALCULATIONS

In the effort to characterize the CFRMF spectrum, transport,
Monte Carlo and resonance theory, computerized techniques have been
applied. The versatility of the transport code (SCAMP, ID, P1, S6)
with its many options and relatively short computation time made it
quite useful for most of the calculations. Monte Carlo calculations
were used to test for smoothing effects in the cross-section pro-
cessing, and only minor differences were observed. The resonance
theory spectrum also showed only minor differences in comparison
with the transport theory in the resonance energy region. Extensive
tests of the cylindrical model to give the best representation of
the complex CFRMF assembly have shown the best compromise between
neutron energy group structure and material regions to be 71 energy
groups with 0.25 lethargy spacing from 21 MeV down. Both cell and
full-core models have been used in the calculations, with only minor
differences resulting. ENDF/B versions III and IV have both been
used, and version IV data produce more relative flux above 0.5 MeV
due primarily to the version IV changes in ^{238}U inelastic scattering.
At this time the recommended spectrum for CFRMF is the full-core
cylindrical model calculation using ENDF/F version IV cross-section
data. This spectrum is tabulated in Table IX. In Figure 7, this
spectrum is compared with a similar spectrum derived using ENDF/B III
data. The spectrum derived from ENDF/B data spectrum is recommended
because it agrees well in shape with the measurements in the energy
regions where the various measurements are considered to be most
credible and because it is impossible to make spectrum measurements
over the entire energy range of interest.

TABLE IX

CFRMF CENTRAL NEUTRON SPECTRUM

SCAMP 75/271

i	U_i	$E_i(eV)$	$\phi(U_i)$	$\int_{U_{i-1}}^{U_i}\phi(U)du$	i	U_i	$E_i(eV)$	$\phi(U_i)$	$\int_{U_{i-1}}^{U_i}\phi(U)du$
0	+.75	2.12×10^7	1.46×10^{-6}	----	-	---	----	----	----
1	-.50	1.65×10^7	3.55×10^{-5}	2.78×10^{-6}	2	.25	1.28×10^7	4.14×10^{-4}	4.10×10^{-5}
3	.00	1.00×10^7	2.52×10^{-3}	2.99×10^{-4}	4	.25	7.79×10^6	1.03×10^{-2}	1.45×10^{-3}
5	.50	6.07×10^6	2.51×10^{-2}	4.26×10^{-3}	6	.75	4.72×10^6	4.66×10^{-2}	8.91×10^{-3}
7	1.00	3.68×10^6	7.07×10^{-2}	1.45×10^{-2}	8	1.25	2.87×10^6	1.01×10^{-1}	2.14×10^{-2}
9	1.50	2.23×10^6	1.24×10^{-1}	2.86×10^{-2}	10	1.75	1.74×10^6	1.35×10^{-1}	3.22×10^{-2}
11	2.00	1.35×10^5	1.63×10^{-1}	3.70×10^{-2}	12	2.25	1.05×10^6	2.07×10^{-1}	4.60×10^{-2}
13	2.50	8.21×10^5	2.67×10^{-1}	5.88×10^{-2}	14	2.75	6.39×10^5	3.24×10^{-1}	7.45×10^{-2}
15	3.00	4.98×10^5	3.28×10^{-1}	8.31×10^{-2}	16	3.25	3.88×10^5	3.16×10^{-1}	7.92×10^{-2}
17	3.50	3.02×10^5	3.03×10^{-1}	7.94×10^{-2}	18	3.75	2.35×10^5	2.64×10^{-1}	7.05×10^{-2}
19	4.00	1.83×10^5	2.11×10^{-1}	6.01×10^{-2}	20	4.25	1.43×10^5	1.90×10^{-1}	4.85×10^{-2}
21	4.50	1.11×10^5	1.52×10^{-1}	4.48×10^{-2}	22	4.75	8.65×10^4	1.34×10^{-1}	3.36×10^{-2}
23	5.00	6.74×10^4	1.19×10^{-1}	3.32×10^{-2}	24	5.25	5.25×10^4	8.37×10^{-2}	2.48×10^{-2}
25	5.50	4.09×10^4	6.38×10^{-2}	1.83×10^{-2}	26	5.75	3.18×10^4	5.82×10^{-2}	1.48×10^{-2}
27	6.00	2.48×10^4	5.06×10^{-2}	1.40×10^{-2}	28	6.25	1.93×10^4	3.38×10^{-2}	1.06×10^{-2}
29	6.50	1.50×10^4	2.75×10^{-2}	7.24×10^{-3}	30	6.75	1.17×10^4	2.58×10^{-2}	6.85×10^{-3}
31	7.00	9.12×10^3	1.93×10^{-2}	5.66×10^{-3}	32	7.25	7.10×10^3	1.62×10^{-2}	4.30×10^{-3}
33	7.50	5.53×10^3	1.49×10^{-2}	3.94×10^{-3}	34	7.75	4.31×10^3	1.56×10^{-2}	3.68×10^{-3}
35	8.00	3.35×10^3	1.44×10^{-2}	3.93×10^{-3}	36	8.25	2.61×10^3	1.15×10^{-2}	3.17×10^{-3}

TABLE IX (cont.)

| i	U_i	$E_i(eV)$	$\phi(U_i)$	$\int_{U_{i-1}}^{U_i}\phi(U)du$	i	U_i	$E_i(eV)$	$\phi(U_i)$	$\int_{U_{i-1}}^{U_i}\phi(U)du$
37	8.50	2.03×10^3	1.18×10^{-2}	2.85×10^{-3}	38	8.75	1.58×10^3	1.13×10^{-2}	2.96×10^{-3}
39	9.00	1.23×10^3	7.92×10^{-3}	2.46×10^{-3}	40	9.25	9.61×10^2	7.35×10^{-3}	1.77×10^{-3}
41	9.50	7.49×10^2	6.44×10^{-3}	1.84×10^{-3}	42	9.75	5.83×10^2	5.65×10^{-3}	1.42×10^{-3}
43	10.00	4.54×10^2	4.40×10^{-3}	1.33×10^{-3}	44	10.25	3.54×10^2	3.17×10^{-3}	8.92×10^{-4}
45	10.50	2.75×10^2	2.70×10^{-3}	7.45×10^{-4}	46	10.75	2.14×10^2	1.97×10^{-3}	5.83×10^{-4}
47	11.00	1.67×10^2	2.04×10^{-3}	4.75×10^{-4}	48	11.25	1.30×10^2	1.01×10^{-3}	4.25×10^{-4}
49	11.50	1.01×10^2	8.91×10^{-4}	1.81×10^{-4}	50	11.75	78.9	5.88×10^{-4}	2.23×10^{-4}
51	12.00	61.4	4.35×10^{-4}	1.02×10^{-4}	52	12.25	47.9	2.99×10^{-4}	1.05×10^{-4}
53	12.50	37.3	1.37×10^{-4}	4.88×10^{-5}	54	12.75	29.0	1.36×10^{-4}	3.29×10^{-5}
55	13.00	22.6	3.94×10^{-5}	2.39×10^{-5}	56	13.25	17.6	2.99×10^{-5}	5.14×10^{-6}
57	13.50	13.7	2.59×10^{-5}	8.77×10^{-6}	58	13.75	10.7	1.06×10^{-5}	4.18×10^{-6}
59	14.00	8.32	1.79×10^{-6}	1.39×10^{-6}	60	14.25	6.48	3.14×10^{-7}	1.86×10^{-7}
61	14.50	5.04	3.72×10^{-7}	8.02×10^{-8}	62	14.75	3.93	1.58×10^{-7}	7.17×10^{-8}
63	15.00	3.06	4.76×10^{-8}	2.23×10^{-8}	64	15.25	2.38	9.68×10^{-9}	6.35×10^{-9}
65	15.50	1.86	1.72×10^{-9}	1.13×10^{-9}	66	15.75	1.44	2.58×10^{-10}	1.98×10^{-10}
67	16.00	1.13	3.41×10^{-11}	2.78×10^{-11}	68	16.25	.876	2.41×10^{-11}	5.98×10^{-12}
69	16.50	.683	2.35×10^{-12}	2.98×10^{-12}	70	16.75	.532	1.21×10^{-13}	1.79×10^{-13}
71	17.00	.414	6.76×10^{-15}	1.01×10^{-14}					

41
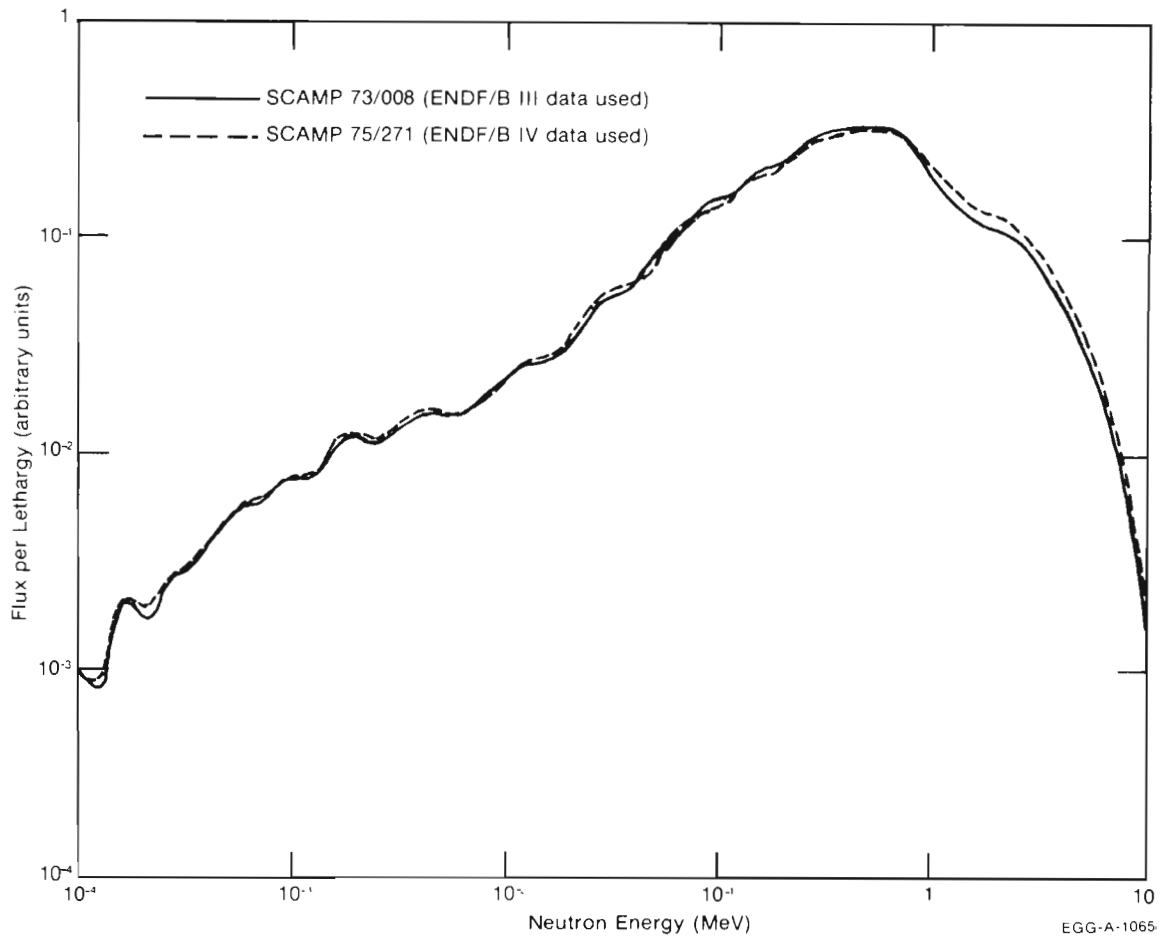
Fig. 7. CFRMF Neutron Spectrum calculated from transport theory.

VII. REFERENCES

1. E. Fast, C. L. Beck, D. A. Millsap, R. G. Nisle, JW Rogers and J. J. Scoville, Use of ARMF for a Fast Reactor Support Program. IN-1143 (November 1967).

2. E. E. Burdick, E. Fast, and D. W. Knight, The Advanced Reactivity Measurements Facilities, IDO-17005 (October 1964).

3. JW Rogers, D. A. Millsap, and Y. D. Harker, CFRMF Neutron Field Flux Spectral Characterization, Nuclear Technology 25, 330 (February 1975).

4. JW Rogers, Y. D. Harker, and D. A. Millsap, "Fast Neutron Spectrum and Dosimetry Studies in the CFRMF, "First ASTM-EURATOM Svmposium on Reactor Dosimetry (September 1975). EUR 5667^e/$_f$, Part II pp 277-298.

5. G. DeLeeuw-Gierts, S. DeLeeuw, H. H. Helmick and JW Rogers, "Neutron Spectromety Data in LMFBR Benchmark and Standard Neutron Fields" First ASTM-EURATOM Symposium on Reactor Dosimetry, (September 1975). EUR 5667 ^{e}/$_f$, Part I pp 99-118

DISTRIBUTION RECORD FOR TREE-1259

Internal Distribution

1 - Chicago Patent Group - DOE
    9800 South Cass
    Argonne, IL   60439

1 - C. A. Benson
    Idaho Operations Office - DOE
    Idaho Falls, ID   83401

1 - H. P. Pearson
    Information Management

10 - INEL Technical Library

20 - Author

External Distribution

93 - Special External

227 - UC 79d, LMFBR-Physics

Total Copies Printed - 353